Received: 2 February 2024 | Revised: 7 June 2024 | Accepted: 17 June 2024

DOI: 10.1002/pip.3832

RESEARCH ARTICLE

PROGRESS IN PHOTOVOLTAICS WILEY

Assessing the accuracy of two steady-state temperature models for onboard passenger vehicle photovoltaics applications

Neel Patel[1] | Bart E. Pieters[1] | Karsten Bittkau[1] | Evgenii Sovetkin[1] | Kaining Ding[1] | Angèle Reinders[2]

[1]IEK5-Photovoltaik, Forschungszentrum Jülich, Jülich, Germany

[2]Energy Technology Group, Eindhoven University of Technology, Eindhoven, The Netherlands

Correspondence
Neel Patel, IEK5-Photovoltaik, Forschungszentrum Jülich, 52425 Jülich, Germany.
Email: n.patel@fz-juelich.de

Funding information
HITEC Graduate School

Abstract

We assess the accuracy of two steady-state temperature models, namely, Ross and Faiman, in the context of photovoltaics (PV) systems integrated in vehicles. Therefore, we present an analysis of irradiance and temperature data monitored on a PV system on top of a vehicle. Next, we have modeled PV cell temperatures in this PV system, representing onboard vehicle PV systems using the Ross and Faiman model. These models could predict temperatures with a coefficient of determination (R^2) in the range of 0.61–0.88 for the Ross model and 0.63–0.93 for the Faiman model. It was observed that the Ross and Faiman model have high errors when instantaneous data are used but become more accurate when averaged to timesteps of greater than 1000–1500 s. The Faiman model's instantaneous response was independent of the variations in the weather conditions, especially wind speed, due to a lack of thermal capacitance term in the model. This study found that the power and energy yield calculations were minimally affected by the errors in temperature predictions. However, a transient model, which includes the thermal mass of the vehicle and PV modules, is necessary for an accurate instantaneous temperature prediction of PV modules in vehicle-integrated (VIPV) applications.

KEYWORDS
PV cell temperature, temperature measurements, temperature modeling, VIPV

1 | INTRODUCTION

Effects of temperature on the operation of conventional photovoltaics (PV) applications in rack-mounted settings have been extensively studied and reported.[1,2] The increased operating temperature of a PV module reduces the operating voltage and, hence, the output power of the PV module, which is accounted for by various temperature coefficients. For a typical silicon-based module, the temperature coefficient of power is −0.35%/°C,[3] which translates to a power drop of 0.35% for a 1-degree increase in temperature. Various modeling approaches have been reported to estimate the PV module temperature in conventional PV applications, ranging from first principles transient model based on the heat transfer approach to steady state one-dimensional empirical approaches.[4–7] Transient models describe the thermal system relatively better at the cost of more computational power and input parameters. In

contrast, the steady-state approach offers a trade-off with less computational power and fewer input parameters at a relatively lower accuracy.

Temperature similarly affects the performance of PV modules in onboard vehicle applications, also known as vehicle-integrated PV (VIPV). However, compared to a stationary PV installation, PV modules onboard vehicles, on the one hand, can rapidly cool down due to the high headwind due to vehicle motion and, on the other hand, strongly heat up during parking due to a lack of ventilation at their rear. Since we are in the infancy of this onboard vehicle PV application, we would like to understand how temperature evolves in such a cyclic operation in two typical modes: driving and parking. Efforts have been ongoing to study the temperature effects in both operation modes. The temperature effects on different PV technologies during the parking phase using an experimental setup of a black box with PV on top to replicate a vehicle cabin were studied in previous studies.[8,9] In their studies, Wheeler et al. utilized the collected data to apply the steady-state temperature model proposed by King et al.,[10] as documented in literature.[8,9] The effects of temperature on the silicon-based modules and their subsequent effect on the PV energy yield in different climatic conditions are described in Yamaguchi et al.[11] In this work, Yamaguchi et al. conducted temperature measurements utilizing a Toyota Prius and a Nissan van for their analysis.[11] The measured data are used to analyze the temperature rise in VIPV applications and empirically determine the model parameters described in King et al.[10] The findings presented by Yamaguchi et al. highlight a significant temperature-induced decrease in the power output of VIPV modules, showing reductions of 16.6% and 31.9% for scenarios in Nagoya and Yokohama, Japan, respectively.[11] The effect of forced convection on the temperature of a PV module on a vehicle while driving was studied in Hayakawa et al.[12] using an experimental setup involving an actual vehicle. Parking a vehicle with onboard PV under the sun will increase the cabin temperature, and the ability of PV energy yield to supply the energy needed to cool the cabin is addressed in Gaspar et al.[13] The studies on temperature modeling of onboard vehicle PV have yet to be comprehensive, with the question of the best approach to perform such modeling being unanswered. More temperature measurements on actual vehicles, in both the driving and parking phase, are needed, along with suitable models to describe temperature in such a dynamic system. We want to address these aspects with a measurement campaign in Germany and use steady-state temperature models to quantify their effectiveness in this application.

The paper is organized as follows: Section 2 describes our data monitoring setup and the monitored data. Section 3 introduces two conventional steady-state PV temperature models, Ross[6] and Faiman,[7] and describes parametrization approaches for the models involved. Section 3 also describes the calculations performed to analyze the impact of model-predicted temperatures on the energy yield. Section 4 presents the model parametrizations' results, accuracy, and effect on energy yield. It also discusses their suitability for temperature modeling for onboard vehicle PV with recommendations for future modeling work. Section 5 concludes the paper.

2 | EXPERIMENTAL

With this paper, we are furthering the research on the temperature modeling of onboard vehicle PV using 1–3 s timestep measurements of PV modules on a car's roof during the parking phase. Furthermore, we measure irradiance, ambient temperature, and wind speed surrounding the car. The monitoring setup used and the monitored data are explained in the following subsections.

2.1 | Monitoring setup

The setup consists of two separate monitoring systems. System 1 monitors position, irradiance, ambient temperature, wind speed, and direction. System 2 monitors temperatures inside the vehicle cabin and the mini PV modules on the vehicle. Both measurement systems can be seen in Figure 1. Sensors used in both systems are mentioned in Table 1.

System 1 consists of sensors and a data logger mounted on an aluminum frame, as shown in Figure 1. Irradiance sensors are mounted on the left, right, up, and front sides. The upward-facing sensor measures the global horizontal irradiation. The system samples data from all the sensors simultaneously every 1–3 s.

System 2 focuses on temperature measurements in and on the vehicle. We use a black Ford Fiesta for our temperature measurements, as seen in Figure 1. Custom-designed mini PV modules with embedded PT100 temperature sensors with a magnetic back are attached to the vehicle's roof to simulate onboard vehicle PV. The minimodules approximate VIPV conditions in which the PV modules are in close contact with the vehicle body, and the system's heat capacity is the combined heat capacity of the PV modules and the vehicle. Four separate PT100s are also placed in the vehicle to measure cabin temperature. We monitor the temperature from eight different PT100s connected to a data logger in a four-wire configuration sampled every second. Since we are just analyzing the suitability of steady-state temperature models in this paper, we only use data from one irradiance sensor, ambient temperature, wind speed, and temperature of one minimodule.

2.2 | Monitored data

The two monitoring systems were deployed at the research center parking place, with both systems being next to each other (see Figure 1). The data were collected in June 2023 for nine weekdays in a time window between 7:00 am and 6:00 pm. The monitored data comprise clear sky, cloudy, and periodic shading conditions from surrounding objects to simulate real parking scenarios. After processing the data from the two monitoring systems, we are left with 122,000 complete measurements with a timestep of 1–3 s and a total measurement duration of around 60 h. Figure 2 shows the measured irradiance on the sky-facing sensor, ambient temperature, wind speed, and temperature of one of the vehicle-mounted mini PV modules.

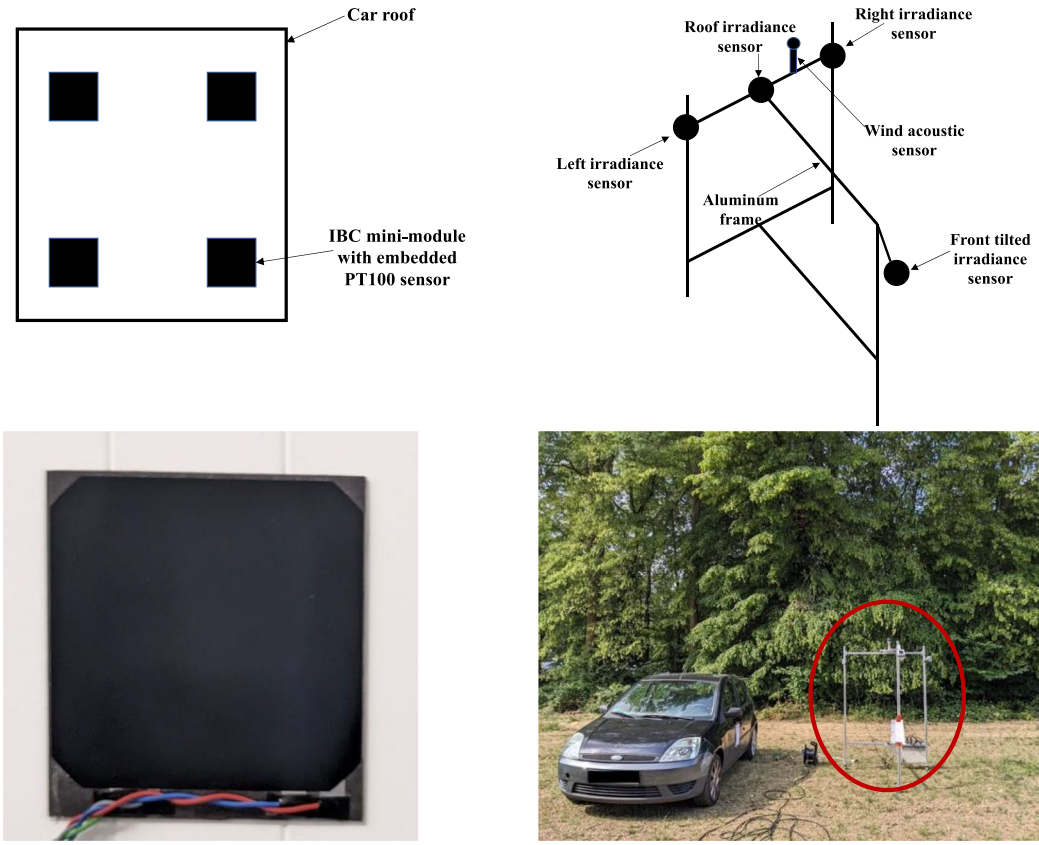

FIGURE 1 Monitoring system setup clockwise from top left: schematic of the minimodules on a vehicle roof, schematic of the irradiance monitoring setup, a vehicle with PT100 sensors inside, and on the vehicle next to the irradiance measurement setup (highlighted red), and picture of a minimodule with integrated PT100 temperature sensor.

TABLE 1 Measured variables, sensors used, and their accuracy.

Variable	Description	Sensor	Sensor accuracy
Irradiance	Irradiance sensor mounted on the aluminum frame facing upwards (roof) (W/m^2)	Si reference cell, Ingenieurbüro Mencke & Tegtmeyer GmbH of type Si-RS485TC-T-MB	±0.4% to ±1.6%
Ambient temperature	Sensor mounted on the aluminum frame at ~2 m height (°C)	Acoustic resonance sensor, FT Technologies Ltd. - FT205EV	±2°C
Wind speed	Sensor mounted on the aluminum frame at ~2 m height (m/s)	Acoustic resonance sensor, FT Technologies Ltd. - FT205EV	±0.3 m/s
Module temperature	Temperature sensor embedded in mini PV modules (IBC cells) on the roof of the vehicle (°C)	Resistance temperature detectors (RTD), PT100	±0.3°C to ±1°C

3 | TEMPERATURE MODELING

The following subsections briefly introduce the models we investigate and their parameterizing procedure.

3.1 | Ross model (NOCT model)

The Ross model represents a linear relationship between the difference of module and ambient temperature with the plane of array (POA) irradiance,[6] as seen in (1). This model is used to determine the nominal operating cell temperature (NOCT) and was part of the old IEC standard with the following conditions: 800 W/m^2 irradiance, 20°C ambient temperature, 1 m/s wind speed, module tilt angle of 37 degrees, and open-air ventilation.

$$T_m = T_a + k \times G_{poa}, \quad (1)$$

where T_m = module temperature (°C), T_a = ambient temperature (°C), k = heat loss coefficient ($°Cm^2/W$), and G_{poa} = plane of array irradiance (W/m^2).

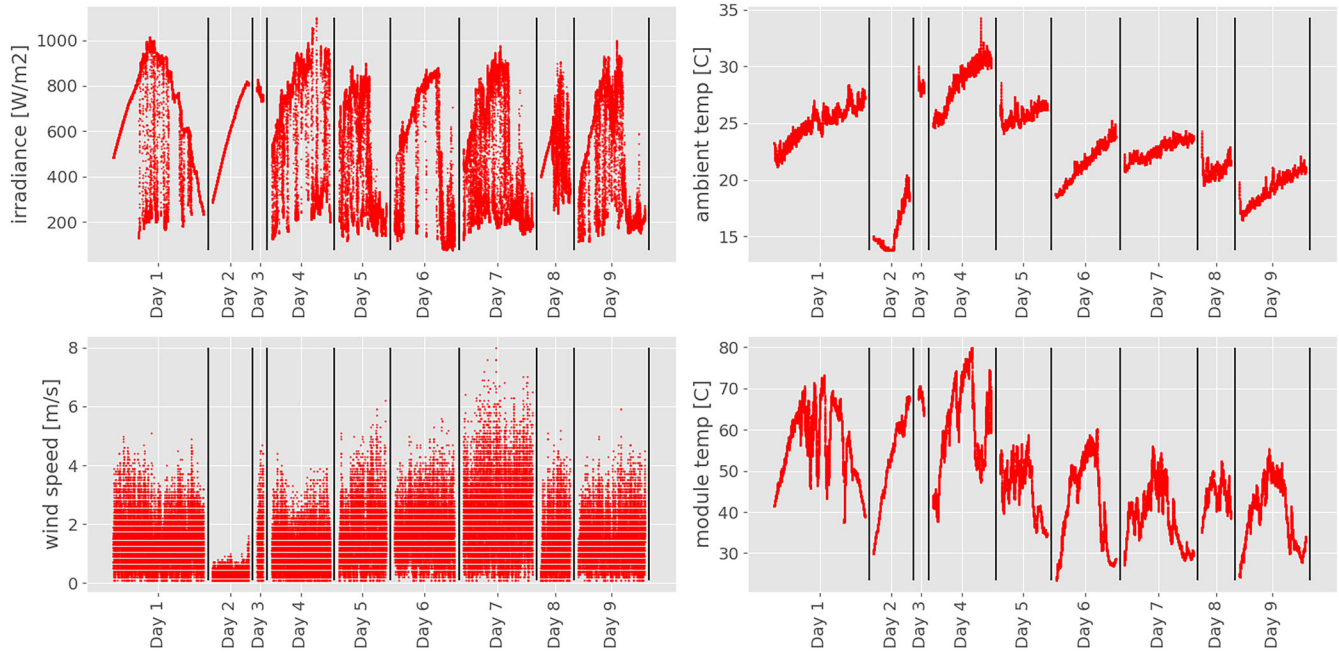

FIGURE 2 Visualizations of the monitored data used in this paper. The y-axis of each subplot indicates the parameter visualized along with respective units. The irradiance shown here is the one measured by the sky-facing sensor. The module temperature is shown from the minimodule on the vehicle's front side.

The constant k defines the thermal characteristic of a module and is determined empirically by a first-order regression.

3.2 | Faiman model (NMOT model)

The Faiman model[7] is an extension of the Ross model with consideration for the wind speed to account for module cooling due to forced convective heat transfer. The Faiman model determines the nominal module operating temperature (NMOT) and is part of the newer IEC standard.[1] The model relationship is seen in (2).

$$T_m = T_a + \frac{G_{poa}}{u_0 + u_1 \times W_s}, \quad (2)$$

where T_m = module temperature (°C), T_a = ambient temperature (°C), G_{poa} = plane of array irradiance (W/m^2), u_0 = thermal loss coefficient (W/m^2°C), u_1 = convective thermal loss coefficient (Ws/m^3°C), and W_s = wind speed (m/s).

We parameterize u_0 and u_1 using the data we measured by applying first-order regression.

3.3 | Model parameterization

Before parameterization, the data need to be filtered per the recommendations in the IEC standards. The filtering requirements are slightly different for both models and are described in Muller et al.[1] and are as follows:

For the Ross model, data with the following conditions were rejected:

- Irradiance below 400 W/m^2
- In a 10-min interval after the irradiance varied by more than 10% from the maximum value to the minimum value recorded during that 10 min period
- Wind speed outside the range of 1 m/s ± 0.75 m/s
- Ambient temperature outside the range 20°C ± 15°C.

For the Faiman model, data with the following conditions were rejected:

- Irradiance below 400 W/m^2
- In a 10-min interval after the irradiance varied by more than 10% from the maximum value to the minimum value during the preceding 10-min period
- In a 10-min interval from a deviation of the instantaneous wind speed to below 0.25 m/s or gusts larger than + 200% from a 5-min running average
- When the 5-min running average was less than 1 m/s or greater than 8 m/s.

We process the data before performing parameterization of both models using three approaches: First, we use the respective IEC data filtering guidelines for each model; second, we do not perform filtering as per the guidelines and use all the data as is; and third, we downsample (data-averaging) our data to logarithmically increasing timesteps. No data are filtered out for the data-averaging approach,

but the data fluctuations are reduced or removed depending on the averaging time step. The results of these parameterization approaches are presented in Section 4.

3.4 | Energy yield

Since energy yield is one of the most common metrics calculated to assess system performance, we estimate it using the Ross and Faiman modeled temperatures. This helps us understand how temperature modeling errors lead to energy yield errors. We derive the energy yield by integrating the module power calculated using the monitored irradiance, ambient temperature, wind speed, minimodule temperature, and various modeled module temperatures. The energy yield calculated using the measured minimodule temperature acts as a reference value to estimate the error in yield calculations that stem from the various modeled temperatures. The energy yield is calculated for a single PV module (from the pvlib-python database) using the CEC single diode model present in pvlib-python.[14] The energy yield results for various modeled temperatures are presented in Section 4.

4 | RESULTS

The temperature modeled by the Ross and the Faiman models using various heat loss coefficients derived from different parametrization approaches is presented. We assess the regression quality for all the approaches using the coefficient of determination (R^2) and the standard error of regression (S). The accuracy of the modeled temperatures is also analyzed using the R^2 metric. Furthermore, we present the comparison of the modeled and reference energy yield. We also discuss the suitability of the presented approaches and potential PV temperature modeling approaches for vehicle applications.

4.1 | Temperature modeling

The parametrization results of the Ross and the Faiman model with the measured data using various approaches are shown in Figure 3. The first value on the X-axis of Figure 3 indicates the fit parameters calculated using the original timestep data (OTS). In contrast, the subsequent values are calculated using data that was averaged using logarithmically increasing time steps up to 3600 s (1 h) without filtering out any data. The fitting was also performed on filtered data using the respective IEC guidelines for both models mentioned in Section 3.

The Ross model coefficient seen in Figure 3 is small for the smaller timesteps but increases as the data are downsampled at a larger timestep. As the data are averaged over a more significant time step, the system's dynamics get smoothed out, leading to a higher heat loss coefficient where the model can explain the temperature variance better. From around the 1000–1500 s time step, the coefficient is stable at approximately 0.0485°Cm^2/W. The heat loss coefficient calculated per the IEC guidelines, about 0.052°Cm^2/W, is shown as a horizontal green line, relatively higher than the other variants.

The Faiman model coefficients u_0 and u_1 are also shown in Figure 3, where the u_1 coefficient represents forced convective heat losses. For the smaller time step, all the heat loss is explained by the u_0 coefficient, with the u_1 coefficient only accounting for a minor fraction. However, as the data are averaged, the u_1 coefficient becomes impactful, indicating a cooling effect due to forced convection. After around 1000–1500 s, the u_0 and u_1 coefficients converge. This indicates that the thermal time constant of this system is around 1000–1500 s. The Faiman model coefficients determined using the IEC guidelines are shown as horizontal yellow lines, solid and dashed for u_0 and u_1, respectively.

Figure 4 shows the quality of regressions for the Ross model on the left side for some of the timesteps. For the Ross model, the fit quality is indicated by the relationship of ($T_m - T_a$) and the G_{POA}.

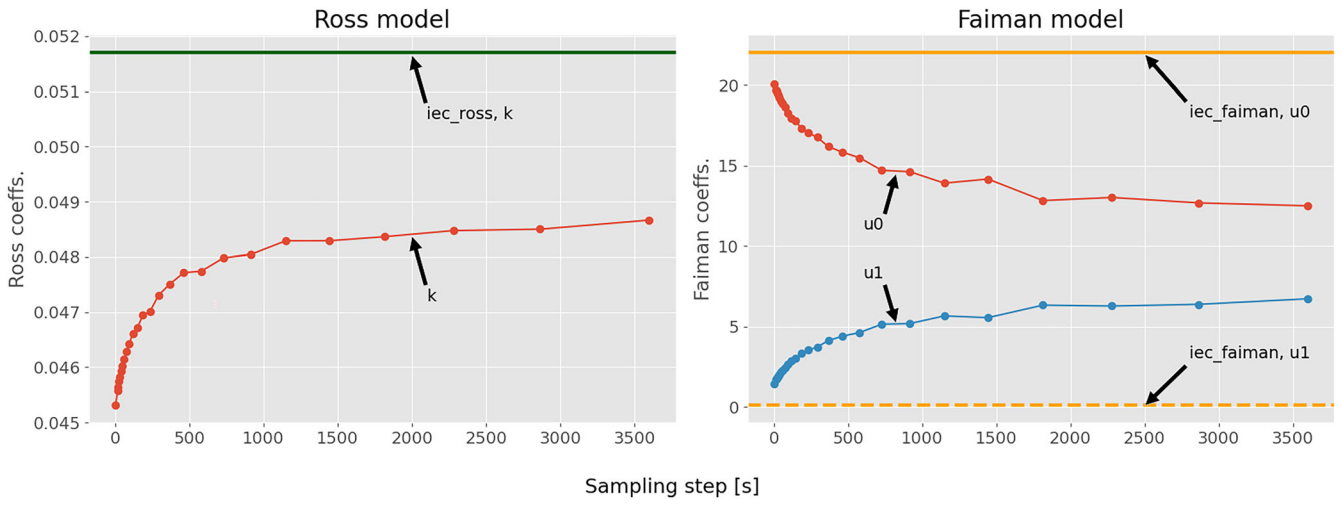

FIGURE 3 Fitting coefficients for the Ross and the Faiman model. The X-axis represents logarithmic time steps used to average the data, with the first value being the original time step. The horizontal lines in both figures indicate the heat loss coefficients derived using the respective IEC filtering guidelines.

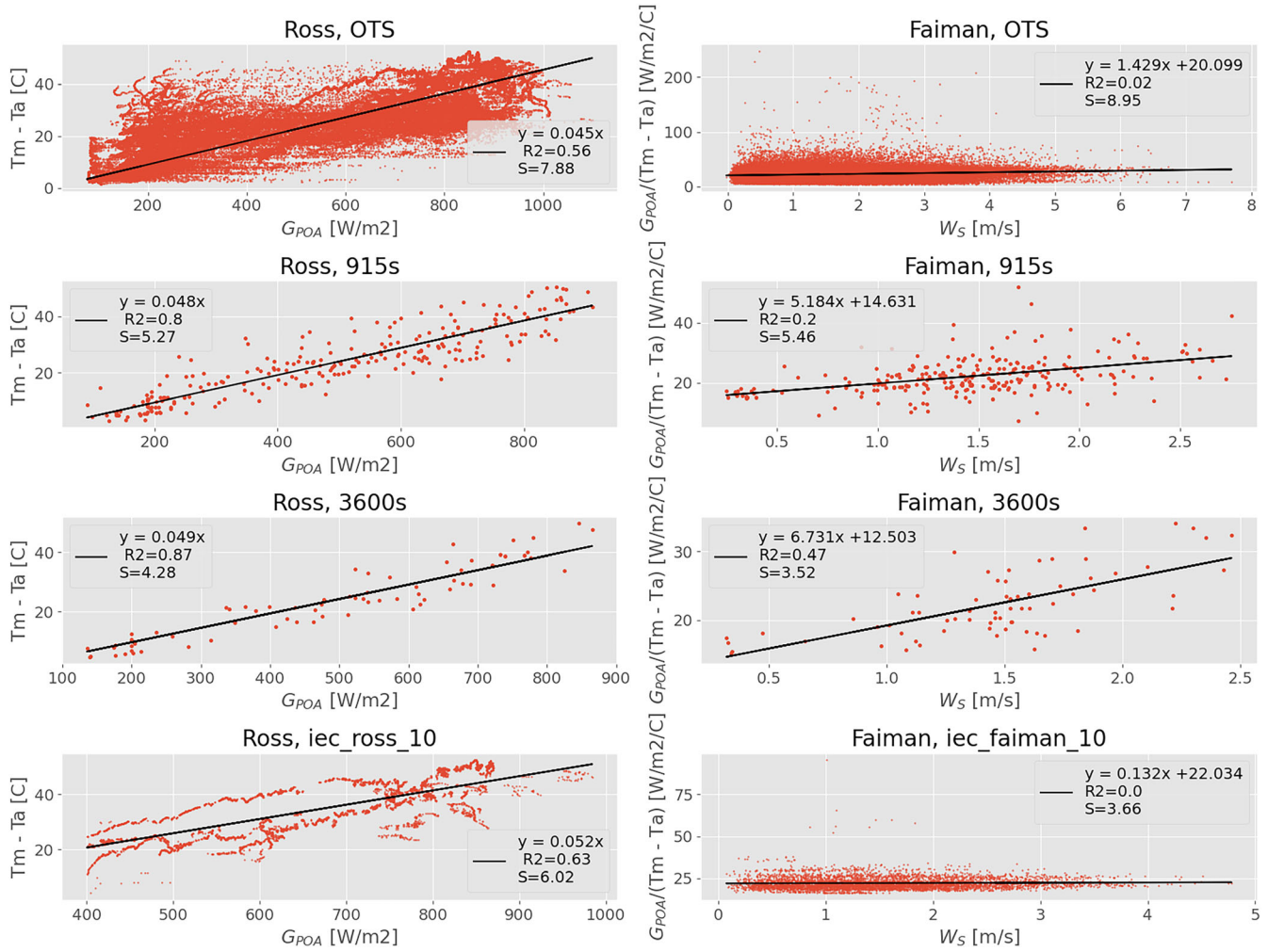

FIGURE 4 Quality of regression fits for the Ross and Faiman models using the data in original (OTS), 915 s, 3600 s time step and the IEC filtered version. The legend indicates the respective calculated heat loss coefficients along with the R^2 and S of the regression fits.

There is a direct correlation between the dependent and the independent variable. The R^2 of the fit is in the range of 0.56–0.87, whereas the standard error of regression (S) is in the range of 4.28–7.88°C. For the original time step (OTS) variant, it is clear from the scatter that the model has difficulty explaining all the variance due to the highly dynamic conditions. However, as the time step is averaged, the scatter becomes focused as the conditions reach a steady state. However, for the IEC version, because most of the data is filtered out to remove abrupt fluctuations, the fit quality suffers, and the model performs worse than the time-averaged version of 3600 s.

Figure 4 also shows the quality of regressions for the Faiman model on the right side for some of the timesteps. For the Faiman model, the fit quality is indicated by the $G_{POA}/(T_m - T_a)$ and wind speed correlation. There is minimal correlation between the dependent and independent variables of the Faiman model. This is indicated by the fit's R^2 value, which ranges from 0.02 to 0.47. However, the correlation is visible as the data are averaged over the 1800 s time step. This is why the u_1 values for the Faiman model are very low for the smaller timesteps and because the cooling effect of the wind is not visible in near-instantaneous data due to the system's thermal mass delaying the effect. Meanwhile, when the data are averaged over a longer time step, the cooling effect becomes visible as the longer time step accounts for the thermal time constant attributable to the system's thermal mass. Most of the data is filtered out for the model fit using the IEC guidelines, leading to skewed coefficients.

The IEC guidelines imply that the thermal time constants for a stationery rack-mounted PV system are 10 min; hence, the requirement of filtering out data in a 10-min window. The time constant for vehicle-mounted PV systems is longer than 10 min, making this filtering method ineffective. So, data in a larger time window need to be thrown away, or it should be averaged. The results presented here suggest that averaging over longer times is a better solution for using a steady-state model for onboard vehicle PV systems.

Figure 5 shows the scatter density plots of the modeled and measured temperature for three parametrization approaches: original time step (OTS) and downsampled variants at 915 and 3600 s. The OTS variant shows a high scatter, showing that the model cannot fully describe the thermal behaviors of the system due to high system dynamics and the system's thermal capacities, which can be seen as distinct trail lines in the scatter plot. The scatter becomes more

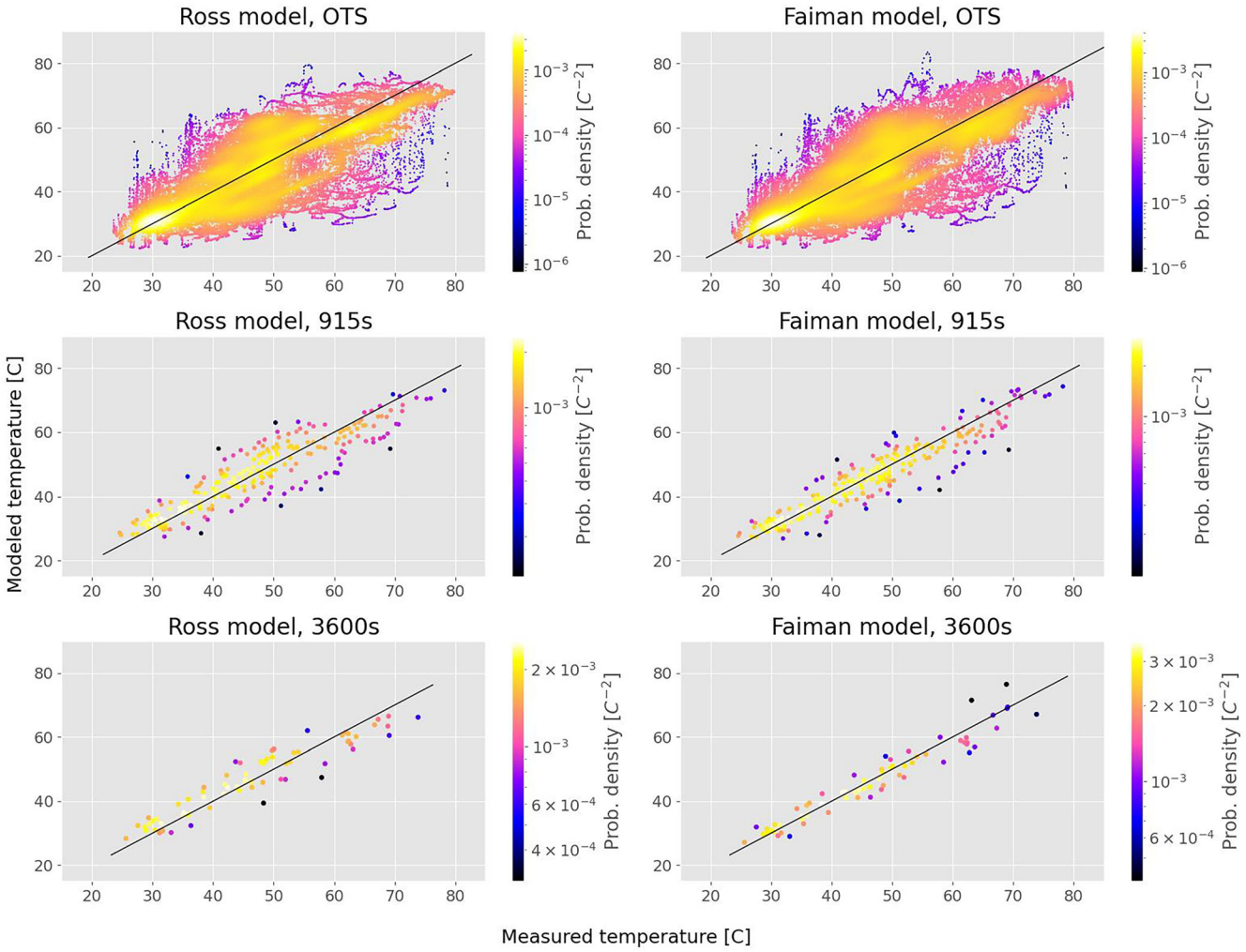

FIGURE 5 Modeled vs. measured temperature using the fitting parameters from OTS, 915 s, and 3600 s data. The color indicates the point density, with bluish being lower and yellowish being higher. As the timestep is averaged, the model performance becomes better. For the OTS variants, the visible trails indicate the thermal time constants involved in the system.

concentrated as we average the data before performing the parametrization, as seen in the plots for 915 and 3600 s. Downsampling reduces the dynamic characteristics of the data by averaging them out. It is expected that the steady-state models will be better able to explain the thermal behavior in less dynamic conditions.

This can also be seen in Figure 6, which shows the R^2 for prediction accuracy of the Ross and the Faiman models for different parameterization approaches. The models perform better for time steps 1000 s and higher, with the Faiman model performing better overall. It is important to note that the R^2 values in Figure 6 are comparable between Ross and Faiman, as both describe the module temperature. However, in Figure 4, the R^2 for Ross is for $(T_m - T_a)$, and for Faiman, it describes $G/(T_m - T_a)$. As the standard deviation of these quantities will differ, so does the R^2 value. Hence, for Figure 4, the R^2 values between the Ross and Faiman models cannot be compared.

The R^2 values for downsampled variants are better than the ones for IEC-filtered variants, as shown by the horizontal lines in Figure 6. This can be attributed to the fact that the data is kept while averaging instead of being thrown away in the IEC filtering approach. However, it is averaged out and still part of the parametrization approach, preserving more detail.

4.2 | Energy yield modeling

The power output was modeled using different modeled temperatures and compared to a reference power output calculated using the monitored temperature for a single PV module. The power output is relatively independent of the modeled temperature errors, with R^2 values close to 1 for all the modeled variants compared to the calculated reference power. We calculated the energy yield by integrating these power outputs for various cases. The relative energy yield, that is, the ratio of calculated energy yield to reference energy yields, is shown in Figure 7. We do not show the relative energy yield for the IEC-filtered data cases as it would be highly inaccurate to calculate

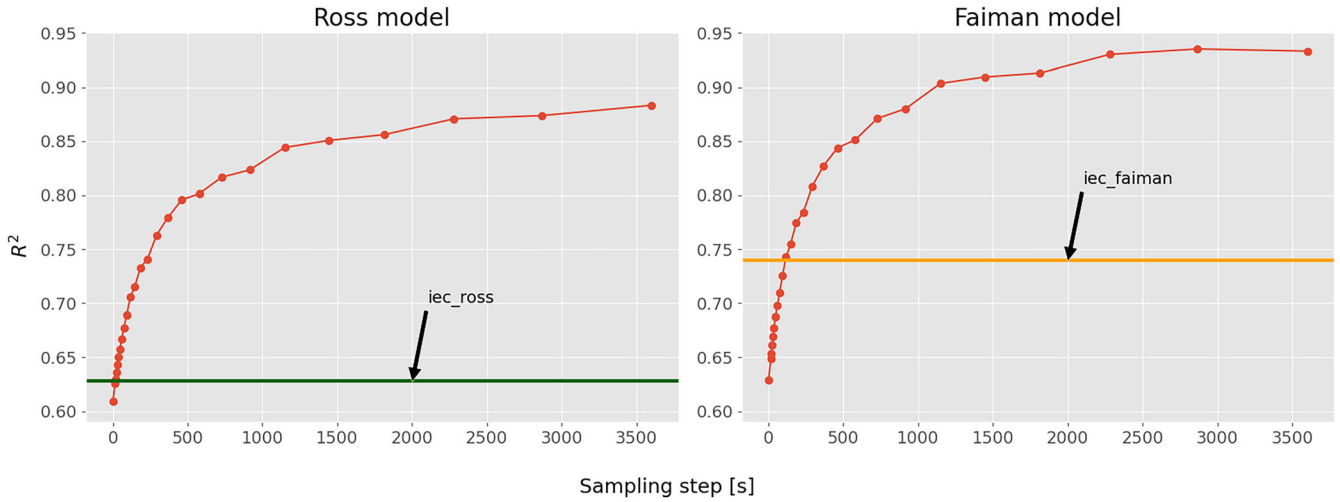

FIGURE 6 R^2 for the predicted temperatures using coefficients determined by various downsampled data variants. Fitting using averaged data at greater than 1000–1500 s timestep performs better (even better than the IEC guidelines, shown as horizontal lines in the respective figures).

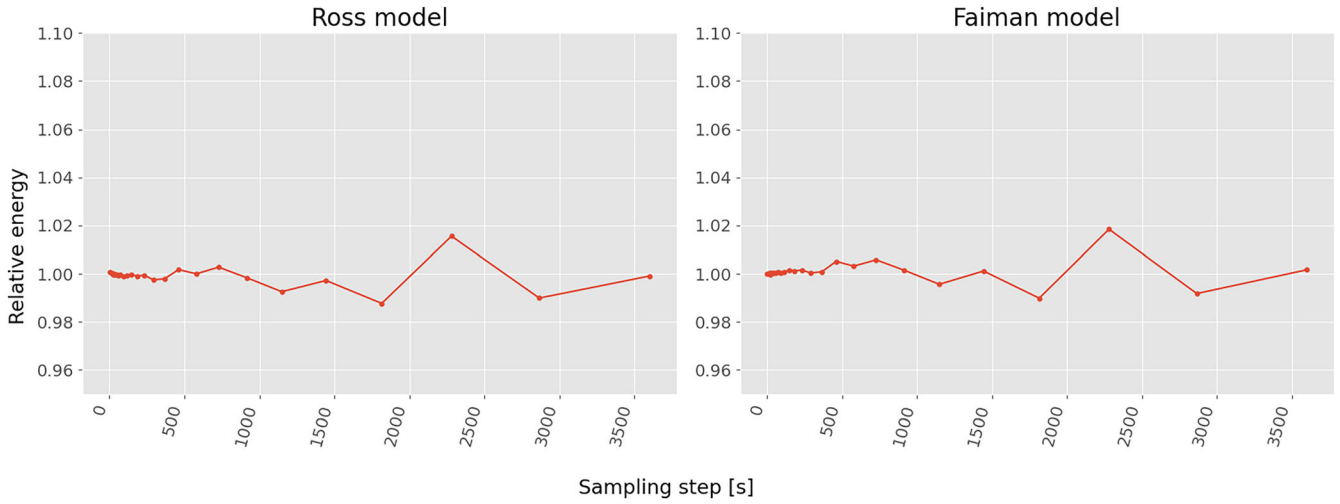

FIGURE 7 Ratio of predicted energy yield with the reference energy yield. For all cases, there is an error of ± 2% or less in energy prediction using various predicted temperatures. IEC-filtered cases are deliberately not shown as estimating energy yield for a time series where most data is filtered out would be difficult.

the energy yield for such a time series where much of the data is missing due to the filtering process. The relative energy yield shows us that energy yield in all cases has an error of ±2% or less in most cases. This highlights that, in this particular case, the accuracy of the energy yield is only mildly affected by the errors in the temperature prediction. However, it is essential to note that this calculation was done for a single module and for a time window of less than 10 days to highlight the impact of temperature on the system's energy yield.

Overall, it can be seen that the Ross and the Faiman models show high errors in predicting instantaneous temperatures, with the magnitude of these errors decreasing as the data are downsampled to 1000–1500 s or longer, with the Faiman model performing relatively better in all considered cases. The primary source of errors in predicting the instantaneous temperatures is the need to consider the thermal capacity of the module as well as the vehicle, which forms a complete system in case of vehicle onboard applications. However, it is also noticeable that errors in temperature prediction do not lead to drastic errors in module power calculations and, hence, the system's energy yield. Using these steady-state temperature models for energy yield predictions over an extended period should be acceptable but is not necessarily accurate enough when the scope changes to instantaneous temperature prediction. Accurate instantaneous temperature prediction (1 s timestep) is essential in optimal system design when various electronic components like optimizers and inverters are part of the system.[15,16] The data collected as a part of this paper will help design transient temperature models that account for the thermal capacity of the module and the vehicle and will be part of a future study.

5 | CONCLUSION

We conducted measurements of temperature and irradiance on a PV module integrated on a vehicle's roof to study their temperature behavior. The measurements were conducted using two specially designed systems with 1–3 s sampling rate for around 60 h. As a first order of measure, we checked the suitability of steady state models, namely, Ross and Faiman, in predicting the temperature in such applications. We used various approaches to parametrize the models. We calculated the k coefficient for the Ross model in the range of 0.045–0.052°Cm^2/W and the u_0 and u_1 coefficients for the Faiman model in the range of 12.5–22 W/m^2°C and 0–6 Ws/m^3°C, respectively. It was determined that due to a lack of thermal capacitance term in the Faiman model, the instantaneous response of the model was independent of the effect of forced convective cooling. We calculated the R^2 values to determine the accuracy of these models, which are in the range of 0.61–0.88 for the Ross model and 0.63–0.93 for the Faiman model, with the Faiman model having an overall better performance. However, the higher values of R^2 for these models are possible only when the data are averaged, indicating that the steady-state models perform better with data at a timestep of around 1000–1500 s or more, which is expected since both models have been developed for simulating stationary PV systems with hourly data resolution. We also checked the impact of the errors in temperature prediction on modeled power output. The R^2 values of comparing modeled power with the reference power were close to 1, indicating that temperature prediction errors have minimal impact on the power prediction. When using these predicted temperatures, energy yield was also calculated to be in the ±2% range compared to the reference value. We conclude that the considered temperature models perform better at time steps greater than 1000–1500 s. Their impact on power/energy yield calculations is minimal in instantaneous or downsampled cases. However, a transient model with the thermal mass of the vehicle and the module is necessary for an accurate instantaneous temperature prediction of PV modules onboard a vehicle. This can be fulfilled in future work by the collected data described in this paper.

ACKNOWLEDGEMENTS

We want to thank Niklas Bongartz, Mohammed Jaber, Wilfried Reetz, Jonas Noll, Christoph Zahren, and Kai Zhang for assisting in procuring and setting up the measurement systems. Open access funding enabled and organized by Projekt DEAL.

DATA AVAILABILITY STATEMENT

Research data are not shared.

ORCID

Neel Patel https://orcid.org/0000-0001-5010-3153
Bart E. Pieters https://orcid.org/0000-0001-6533-2098

REFERENCES

1. Muller M, Marion B, Rodriguez J. "Evaluating the IEC 61215 Ed.3 NMOT procedure against the existing NOCT procedure with PV modules in a side-by-side configuration" in *2012 38th IEEE Photovoltaic Specialists Conference*, IEEE, Jun. 2012, pp. 697–702. 10.1109/PVSC.2012.6317705.
2. Barykina E, Hammer A. "Modeling of photovoltaic module temperature using Faiman model: sensitivity analysis for different climates" *Sol Energy*, vol. 146, pp. 401–416, Apr. 2017, 10.1016/j.solener.2017.03.002.
3. "Solbian solar SP series." [Online]. Available: https://solbian.solar/wp-content/uploads/2019/03/Datasheet-SP.pdf
4. Torres Lobera D, Valkealahti S. "Dynamic thermal model of solar PV systems under varying climatic conditions" *Sol. Energy*, vol. 93, pp. 183–194, Jul. 2013, 10.1016/j.solener.2013.03.028.
5. Barry J, Böttcher D, Pfeilsticker K, et al. "Dynamic model of photovoltaic module temperature as a function of atmospheric conditions" *Adv Sci Res*, vol. 17, pp. 165–173, Jul. 2020, 10.5194/asr-17-165-2020.
6. Ross RG. "Interface design considerations for terrestrial solar cell modules". Presented at the 12th IEEE Photovoltaic Specialists Conference, Baton Rouge Louisiana, 1976.
7. Faiman D. "Assessing the outdoor operating temperature of photovoltaic modules" *Prog Photovolt Res Appl*, vol. 16, no. 4, pp. 307–315, Jun. 2008, 10.1002/pip.813.
8. Wheeler A, Leveille M, Anton I, Leilaeioun A, Kurtz S. "Determining the Operating Temperature of Solar Panels on Vehicles" In *2019 IEEE 46th Photovoltaic Specialists Conference (PVSC)*, IEEE, Jun. 2019, pp. 3592–3597. 10.1109/PVSC40753.2019.9311292.
9. Wheeler A, Leveille M, Anton I, Limpinsel M, Kurtz S. "Outdoor Performance of PV Technologies in Simulated Automotive Environments" In *2019 IEEE 46th Photovoltaic Specialists Conference (PVSC)*, IEEE, Jun. 2019, pp. 3103–3110. 10.1109/PVSC40753.2019.8981352.
10. King D, Boyson W, Kratochvil J. "Photovoltaic array performance model" *SAND2004–3535*, 919131, Aug. 2004. 10.2172/919131.
11. Yamaguchi M, Ota Y, Masuda T, et al. Analysis for effects of temperature rise of PV modules upon driving distance of vehicle integrated photovoltaic electric vehicles. *Energy Power Eng*. 2024;16(4):131-150. doi:10.4236/epe.2024.164007
12. Hayakawa Y, Sato D, Yamada N. "Measurement of the convective heat transfer coefficient and temperature of vehicle-integrated photovoltaic modules" *Energies*, vol. 15, no. 13, p. 4818, Jun. 2022, 10.3390/en15134818.
13. Gaspar G, Costa I, Centeno Brito M. "The parking dilemma for solar-powered vehicles" *Heliyon*, vol. 10, no. 5, p. e26966, Mar. 2024, 10.1016/j.heliyon.2024.e26966.
14. Holmgren WF, Hansen CW, Mikofski MA. "Pvlib python: a python package for modeling solar energy systems," *J Open Source Softw*, vol. 3, no. 29, p. 884, Sep. 2018, 10.21105/joss.00884.
15. Burger B, Rüther R. "Inverter sizing of grid-connected photovoltaic systems in the light of local solar resource distribution characteristics and temperature" *Sol. Energy*, vol. 80, no. 1, pp. 32–45, Jan. 2006, 10.1016/j.solener.2005.08.012.
16. Luoma J, Kleissl J, Murray K. "Optimal inverter sizing considering cloud enhancement" *Sol. Energy*, vol. 86, no. 1, pp. 421–429, Jan. 2012, 10.1016/j.solener.2011.10.012.

How to cite this article: Patel N, Pieters BE, Bittkau K, Sovetkin E, Ding K, Reinders A. Assessing the accuracy of two steady-state temperature models for onboard passenger vehicle photovoltaics applications. *Prog Photovolt Res Appl*. 2024;32(11):790-798. doi:10.1002/pip.3832